PERGAMON

International Journal of Impact Engineering 25 (2001) 423–437

INTERNATIONAL JOURNAL OF IMPACT ENGINEERING

www.elsevier.com/locate/ijimpeng

Impact of the 7.62-mm APM2 projectile against the edge of a metallic target

Sidney Chocron[1], Charles E. Anderson Jr.*, Donald J. Grosch, Carl H. Popelar[2]

Engineering Dynamics Department, Southwest Research Institute, P.O. Drawer 28510, San Antonio, TX 78228-0510, USA

Received 25 January 2000; received in revised form 23 June 2000; accepted 24 October 2000

Abstract

The core of the 7.62-mm, armor-piercing APM2 projectile is very strong, but also brittle. A combined analytical, numerical and experimental investigation examined the conditions to fracture the core. The analytical model is based on a Timoshenko beam analysis, where the projectile is idealized as a semi-infinite cylinder. A 3-D numerical model of the core, impacting against the edge of a metallic plate, was then used to investigate transient effects, the influence of constitutive model assumptions, and the influence of target properties on the magnitude of projectile bending strains. Results are then compared to experimental data. Numerical simulations of the full (jacketed) projectile were also investigated, and it is demonstrated that the erosion strain of the jacket is a critical parameter for successful simulations.

Keywords: Fracture; Armor-piercing; APM2; Timoshenko beam analysis; 3-D numerical simulations; Strain to failure

1. Introduction

Bending stresses are induced in a projectile when it impacts an edge, i.e., periphery, of a target element. If the bending stresses are sufficiently large, the projectile will fracture. This could have an application in the design of lightweight armors since a broken projectile is considerably easier to defeat. The objective of this research effort was to understand the conditions for projectile fracture. An ancillary objective was to determine the optimum plate thicknesses (aluminum or steel) that

* Corresponding author. Tel.: + 1-210-684-5111; fax: + 1-210-522-6092.
E-mail address: canderson@swri.edu (C.E. Anderson Jr.).
[1] Present address. Dpto. Ciencia de Materiales, E.T.S.I. Caminos, Madrid 28040, Spain.
[2] Present address: 602 Stone Wood Dr., San Antonio, TX 78216, USA

0734-743X/01/$ - see front matter
PII: S0734-743X(00)00063-4

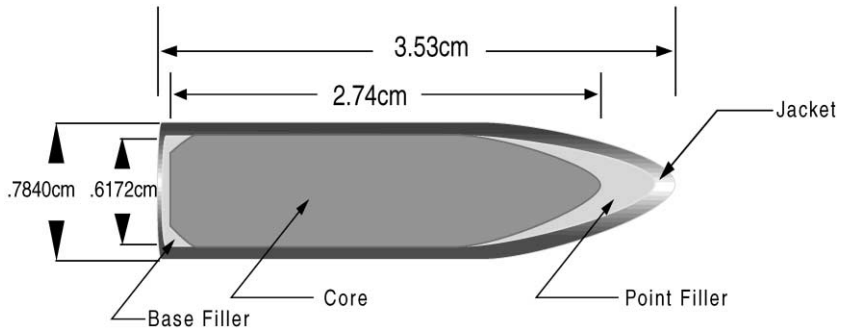

Fig. 1. Schematic of the 7.62-mm APM2 projectile.

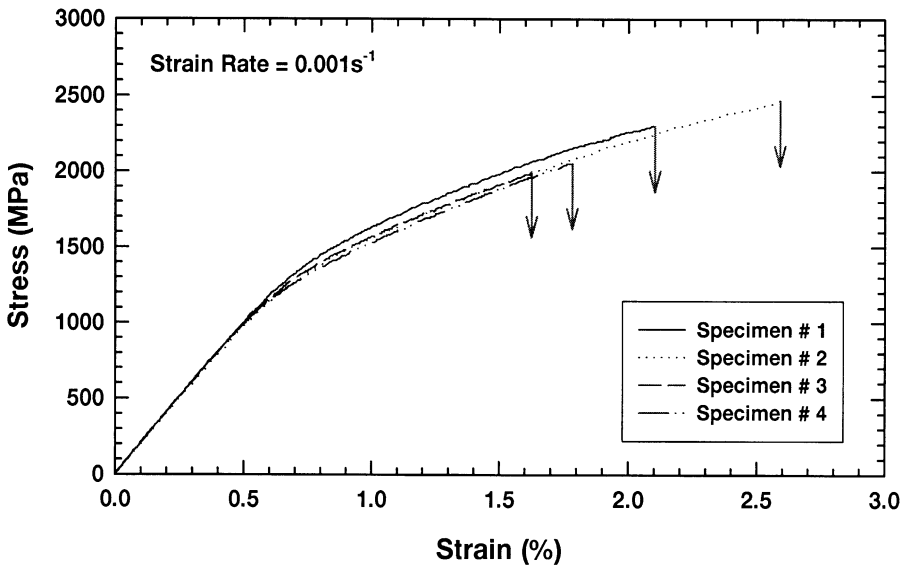

Fig. 2. Stress–strain response of APM2 core material.

would defeat (fracture) the projectile. With this in mind, the edge impact problem was approached in three complementary studies: analytical, numerical, and experimental.

A schematic of the 7.62-mm (0.30-cal), APM2 projectile, with dimensions, is shown in Fig. 1. The projectile consists of a jacket made of gilding material, a lead nose element, lead base filler, and a very hard steel (R_c62) core. The steel core gives the APM2 projectile its strong penetration capability.

The quasi-static stress–strain response was measured for the steel core material. Tensile specimens were fabricated, instrumented with strain gauges, and strained until failure. The test results are plotted in Fig. 2. The vertical arrows denote the total strain at failure; the tails of the arrows denote the stress at failure. It was found that the core material fails at approximately 2% strain at a stress of 2.3 GPa. However, there is variation in the strain to failure and associated ultimate stress.

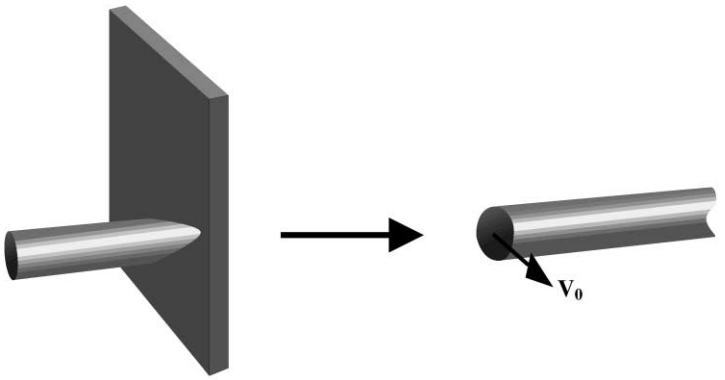

Fig. 3. Equivalence assumed between the real problem and the analytical model.

2. Analytical model

Many simplifications are required to make the edge impact problem tractable to an analytical investigation. First, the projectile will be treated as a semi-infinite, elastic, cylindrical rod. If the maximum flexural strain in the projectile occurs before the time it takes a wave to propagate the length of the projectile and return, then the semi-infinite approximation should be acceptable. Second, at impact, the axis of the projectile is normal to the plate and coincident with its edge (or periphery). This asymmetric loading of the projectile nose imparts a lateral impulse to the projectile. The subsequent transverse motion of the projectile is a dynamic Timoshenko beam. This approximation allows the use of the solution to the dynamic Timoshenko beam equations developed by Boley and Chao [1]. The boundary condition also needs to be simple enough to be analytically tractable, but it should be as close as possible to the condition of edge impact. The boundary condition selected is one where a lateral velocity V_0 is imparted to the end of the cylinder, as shown in Fig. 3. The Timoshenko beam equations, with this boundary condition, were solved to provide the strain history in the cylindrical beam. For the analysis, the rod (projectile) is steel with a density 7850 kg/m^3, bulk modulus 167 GPa, and shear modulus of 76.75 GPa. It is assumed that the response of the cylinder is linearly elastic.

Boley and Chao expressed the solution of the problem in terms of two integrals [1]. The first integral governs the propagation of a flexural wave at the longitudinal bar wave speed $c_1 = (E/\rho)^{1/2}$ where E is the elastic modulus and ρ the mass density. The second integral evaluates the propagation of a slower lateral shear wave at a speed $c_2 = (kG/\rho)^{1/2}$ where G is the elastic shear modulus and k is the shear coefficient. For a circular cross section, Cowper [2] relates k to Poisson's ratio v by Eq. (1). The two integrals then depend upon the single parameter γ as defined by Eq. (2).

$$k = \frac{6(1+v)}{7+6v}, \tag{1}$$

$$\gamma \equiv \frac{E}{Gk} = \frac{7+6v}{3}. \tag{2}$$

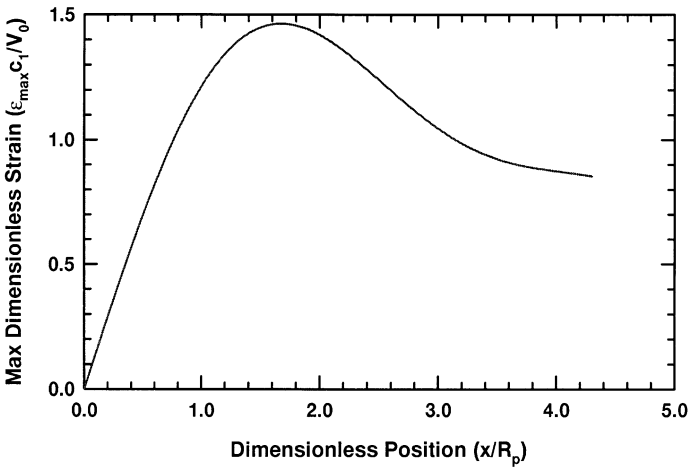

Fig. 4. Predictions of maximum strains from analytical model.

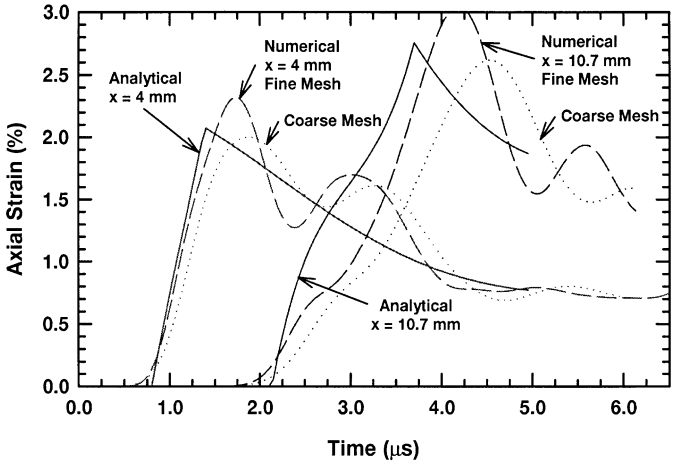

Fig. 5. Comparison of the strains calculated analytically and numerically.

The integrals must be numerically evaluated; $v = \frac{1}{3}$ was used in performing the evaluations.

The maximum scaled strain as a function of scaled distance along the cylinder is shown in Fig. 4. In the figure, the ordinate is the maximum normalized bending strain, and the abscissa is the distance along the cylinder normalized by the projectile radius R_p. The analytical model predicts that the maximum bending strain attains its peak value at a distance of approximately $1.6R_p$.

The maximum bending strain is proportional to the lateral tip velocity V_0. Assuming that $V_0 = 100$ m/s, the axial strains as a function of time at a distance of 4.0 and 10.7 mm from the end of the cylinder are shown in Fig. 5. The figure also shows the solutions for the finite difference numerical simulation, discussed in the next section. For this problem, the peak flexural strain is approximately 3%. A lateral velocity $V_0 = 68$ m/s produces a maximum strain of 2% in the beam,

and from Fig. 2, a strain of approximately 2% is the maximum tensile strain that the core material can support. Therefore, based upon this simple model, it appears that imparting a lateral velocity of about 68 m/s to the tip of the core is sufficient to break the core. Note that this lateral velocity is small compared to the muzzle velocity (approximately 850 m/s) for a typical armor piercing round.[3]

3. Three-dimensional (3-D) numerical simulations

The impact of the APM2 against the edge of a target is a 3-D problem. The numerical code AUTODYN-3D [3] was used to conduct a numerical study of such an impact. Since 3-D calculations require considerable resources, it was decided to simulate first the highly idealized geometry of the analytical model. In this manner, questions dealing with grid resolution and how to analyze and interpret the 3-D results could be investigated and resolved. Then, the real problem could be simulated, thereby extending the results of the simplified analytical model to a more realistic simulation of the actual projectile and impact.

3.1. Numerical model of the analytical problem

A numerical model of a long, right-circular cylinder was generated in AUTODYN-3D. The impact end of the cylinder was given the simple velocity boundary condition used in the analytical analysis. The other end of the projectile is traction free. This problem is symmetric in one plane, so only half of the cylinder needed to be simulated.

Two meshes were used in the numerical calculations: a coarse mesh (4600 elements), and a fine mesh (26,000 elements). The strain histories as a function of time were computed at several positions along the cylinder. It was assumed that the steel core was linearly elastic, with the same properties as in the analytical study (no yield or failure criterion was used in this simulation). The diameter of the cylinder was taken to be 10 mm, and the length was 25 mm, i.e., the projectile is finite in the numerical simulation. The lateral velocity V_0 at the tip of the cylinder was 100 m/s.

The analytical and numerical results are compared in Fig. 5. The strains for the elements closest to the analytical points of 4.0 and 10.7 mm were monitored. Two-dimensional (2-D) transient effects are contained in the numerical solution that are not included in the analytical solution, specifically, radial inertia effects. The numerical solution exhibits some oscillations; radial inertia and other effects (e.g., distortion of the cross section) produce oscillations in the numerical solution that are not present in the simplified analytical solution. These effects result in a slight overshoot of the maximum strain. The overshoot and oscillatory behavior are related to the familiar Pochhammer-Chree oscillations observed in split-Hopkinson pressure bar experiments [4]. As is usual for

[3] The transverse velocity imparted to the projectile is a function of nose shape and where/how the bullet impacts the edge of the plate, as will be shown in the numerical simulations. The analytical model provides an estimate of the required loading conditions to achieve fracture, not how to achieve that loading condition. In the experiments, the impact point can be controlled only to within half a bullet diameter. For the limited number of experiments, the results do not show an influence on the exact impact location.

transient numerical simulations, the rise time is less steep than for the analytical solution; the fine-zone simulation has a steeper rise time than the coarse-zone simulation, as expected. Taking these factors into account, the fine-mesh solution is in better agreement with the analytical solution than the coarse-mesh solution at the 4-mm location. The 2-D transient effects result in more dispersion of the propagating wave than predicted in the analytical solution as the effect of the initial boundary condition propagates along the cylinder. This is clearly evident in a comparison of the solutions at 10.7 mm. Again, it is felt that a more accurate representation of the relevant mechanics is provided by the fine-mesh solution than by the coarse-mesh solution. Now, the impact of the core against the edge of a target will be explored.

3.2. Numerical model of the core of the APM2 impacting the edge of a target

The idealized problem has an applied, instantaneous, transverse velocity at the end of a cylinder. The real problem involves the APM2 projectile striking the edge of a target that has a finite thickness. Thus, the surface of the core, along some portion of its length, is given a transverse velocity during edge impact. Further, this transverse velocity will have gradients, and is not imparted instantaneously. Therefore, the loading history is much more complicated in the real situation than assumed in the above analysis.

Initial 3-D simulations were conducted for the impact of the APM2 core against 6.35-mm thick targets of aluminum and steel. The nominal dimensions of the core, Fig. 1, were used to model the projectile, although the exact details of the ogival nose were approximated. The core was modeled as elastic (since the strain to failure is low for the APM2 core, this assumption provides a reasonable, but conservative, approximation for the strains). The aluminum target was modeled as elastic, perfectly plastic, with the following properties: density $\rho = 2710\,\mathrm{kg/m^3}$; bulk modulus $K = 72.8\,\mathrm{GPa}$; shear modulus $G = 27.3\,\mathrm{GPa}$; yield strength $Y = 380\,\mathrm{MPa}$; and erosion strain = 150%. The initial configuration is shown in Fig. 6(a). Geometrically, it was assumed that the projectile "overlapped" the edge of the target plate by one projectile radius. Again, the projectile is unconstrained and free to rotate as dictated by the dynamics of the problem.

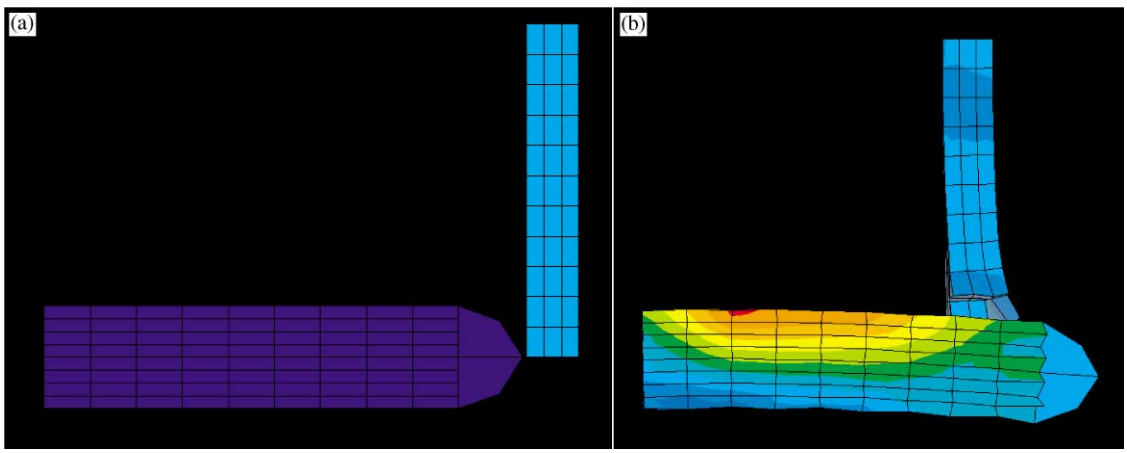

Fig. 6. (a) Initial configuration and (b) stress contours for core 12 μs after impacting edge of target.

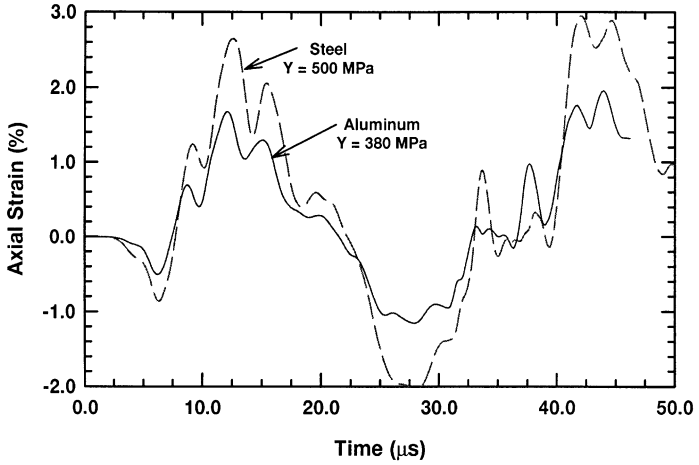

Fig. 7. Strain histories in the element of maximum strain (6.35-mm-thick target).

The initial projectile velocity was 850 m/s. The colors denote stress contours, with the darker blue colors denoting compression, and the orange/red colors denoting tension. The largest tensile stresses correspond to axial strains of approximately 2%. The analytical model predicting the maximum strains were approximately $1.6R_p$ from the end of the cylinder. For the real impact case, it was found that the maximum strains occur approximately in the center edge of the projectile ($\sim 4R_p$), as shown in Fig. 6(b). Contrasting Figs. 5 and 7, the time to achieve maximum strain is considerably longer for the actual impact since there is an interaction time to impart a lateral velocity to the core material. The lateral velocity in the tip of the projectile is not a constant, but varied between approximately 80 and 120 m/s.

The maximum axial strain versus time for a 6.35-mm thick steel target ($\rho = 7850\,\mathrm{kg/m^3}$; $K = 167\,\mathrm{GPa}$; $G = 76.75\,\mathrm{GPa}$; yield strength $Y = 500\,\mathrm{MPa}$, and erosion strain = 150%) is also shown in Fig. 7. This strain induced in the projectile is considerably larger from interaction with the steel plate than for the aluminum plate. To separate and understand the influence of strength and inertial (plate density) effects, additional simulations were conducted. Results are shown in Fig. 8 for a 3.175-mm thick target. The flow stress for the aluminum target was varied from 380 to 500 MPa. The strains are approximately 10% larger for the larger flow stress. In contrast, the strains are 60% larger for the steel plate than for the aluminum plate when the flow stress is held constant at 500 MPa. Thus, it is concluded that plate density has a major effect on the induced strains.

As previously noted, the core was modeled as linearly elastic in the numerical simulations. To verify that this is an adequate approximation, a simulation was performed to evaluate this assumption. Johnson [5] estimated the coefficients for the Johnson–Cook (J–C) viscoplastic constitutive model [6] based on the stress–strain test data in Fig. 1. A target flow stress of 1400 MPa was used in the simulation since this is a reasonable estimate of the flow stress for the hard steel plates used in the experiments (discussed later). The results are compared in Fig. 9. The strain histories are very similar, with the J–C solution reaching a maximum strain 6% less than

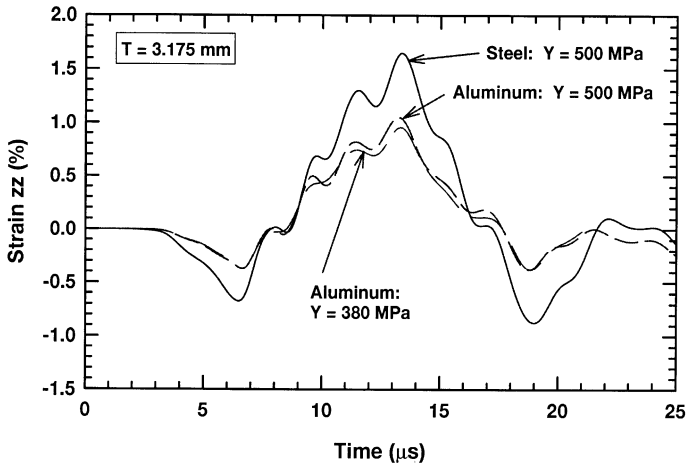

Fig. 8. Comparison of induced strains as a function of plate material.

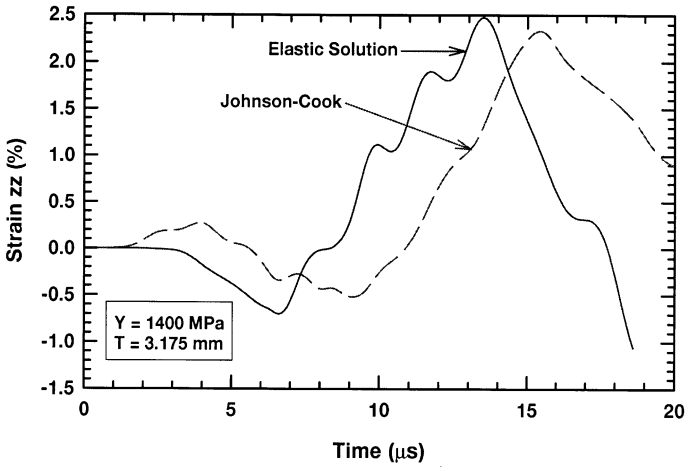

Fig. 9. Induced strains as a function of the assumed constitutive response.

the elastic solution, at approximately 2 μs later in time. Thus, the results using a linear elastic model for the APM2 core are considered a reasonable approximation for the current modeling effort.

It was shown in Fig. 8 that a small change ($\sim$ 25%) in target flow stress had little effect on the induced strain. However, it is expected that larger changes in plate strength should have a significant influence, as can be inferred from comparing the maximum strains in Figs. 8 and 9. Holding the plate thickness constant at 6.35 mm, the flow stress was varied by a factor of three; the results are shown in Fig. 10. As the flow stress is increased from 500 to 1500 MPa, the maximum strain increases by 60% (2.5–4.0%). A series of simulations was next conducted to determine the maximum axial strains as a function of plate thickness, holding the plate flow stress constant. These

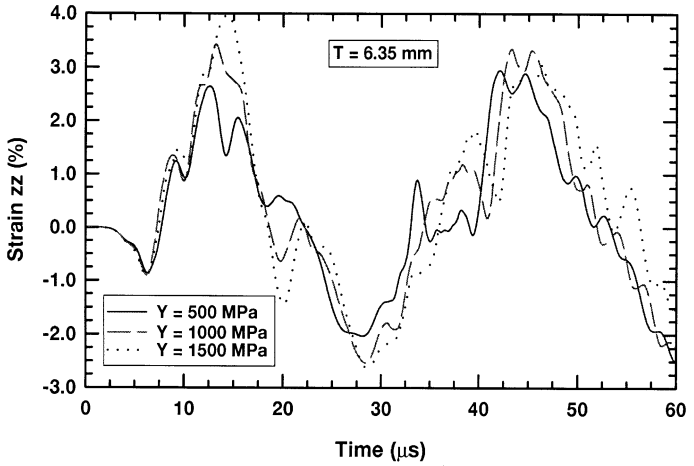

Fig. 10. Strain history as a function of target strength.

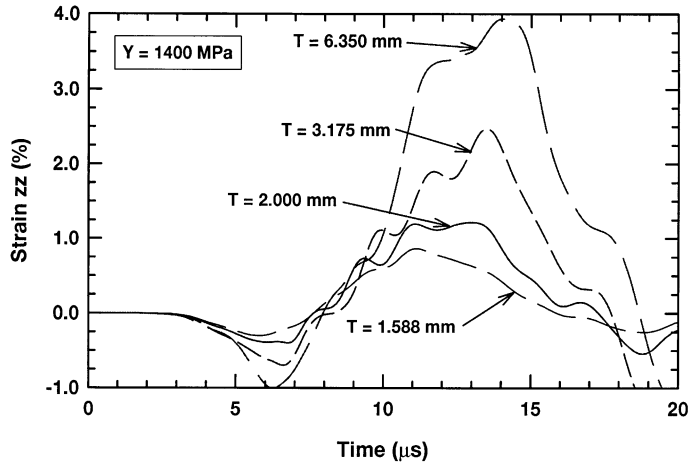

Fig. 11. Strain history as a function of target thickness.

results are plotted in Fig. 11. It is observed that the induced strain increases with plate thickness. The induced maximum is less than 2.5% when the thickness of the 1400-MPa steel plate is less than 3.175 mm.

The results of the simulations for aluminum and steel plates as a function of plate thickness and flow stress are plotted in Fig. 12. In the context of the analytical model, we conclude that increases in plate thickness and/or plate strength (flow stress) increases the lateral velocity imparted to the projectile, with an attendant increase in the maximum bending strain. The numerical results indicate that a steel plate less than 3-mm thick likely would not fracture the core since the maximum induced strain is below 1.5%. Before discussing these computational results as they relate to the experiments, simulations of the full APM2 projectile (with lead nose and jacket) will be described.

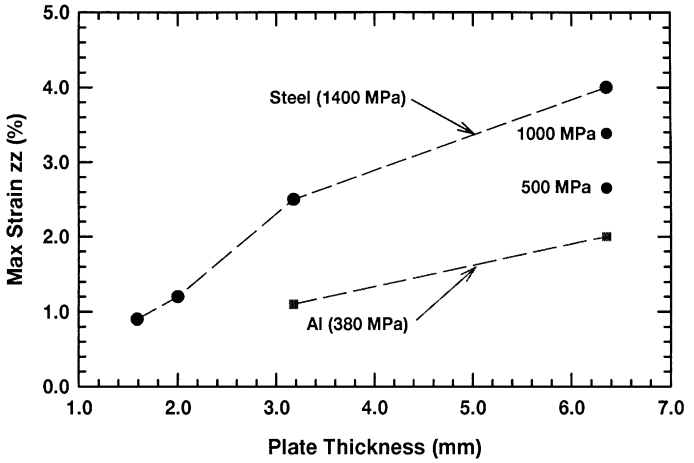

Fig. 12. Maximum strain in the projectile vs. target thickness.

3.3. Numerical model of the full projectile

The numerical simulations described above, although 3-D in nature, modeled only the hard steel core. The APM2 projectile is considerably more complicated, as is shown in Fig. 1. Numerical simulations of the full projectile (including core, lead nose, and jacket) were performed. It was found that there were a number of subtle, and not so subtle, numerical issues. AUTODYN-3D employs a Lagrangian mesh and an erosion strain (for example, see Ref. [7]) must be specified for each material to prevent excessive mesh distortion and mesh entanglement. The erosion strain is distinct from the failure strain. When a computational element exceeds the failure strain, the element is no longer able to support tensile or shear stresses, but the element is still present within the computational mesh and it can support compressive stresses. When an element exceeds the erosion strain, the element is discarded (and depending upon a user option, the element mass is discarded or is concentrated at a node point). It was found that the numerical results for the edge impact problem were very sensitive to the erosion strain.

The full simulation was done for the 3.175-mm-thick steel target. The steel plate, jacket, and lead were considered to be elastic, perfectly plastic; the Johnson–Cook model was employed for the projectile's core. The flow stress for the lead was set at 6 MPa, and that of the jacket material was set to 100 MPa.[4] The initial simulations did not predict failure of the core (i.e., the induced strains

[4] After these simulations were conducted, we characterized the quasi-static stress-strain response for the gilding (jacket) metal. Originally, it was thought that the jacket material would have a response similar to copper, and it was modeled this way in the present study. It was ultimately found that the gilding metal is considerably stronger than copper, having a flow stress of approximately 500 MPa. However, a stronger jacket would have exacerbated the problem that is described in the text.

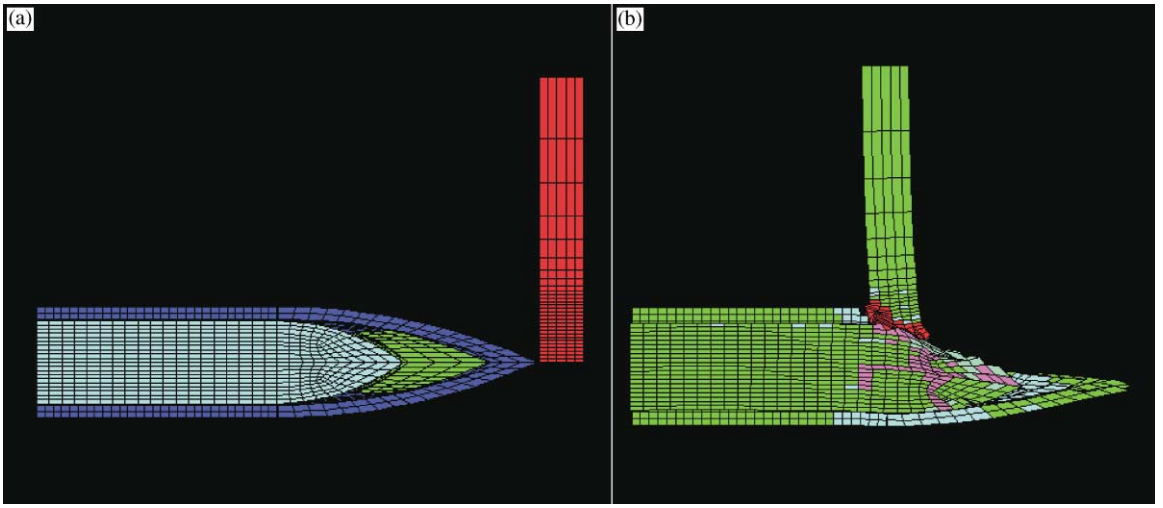

Fig. 13. Model for the full APM2 projectile; (a) initial configuration; (b) deformation at 24 μs.

did not exceed 2%). Examination of the computational results showed that the core was not coming into contact with the plate. A parameter study—where the parameters were varied over a very large range—of several of the input variables was performed. For example, the strength of the target plate was varied from 1.5 to 6.0 GPa. Even when the plate was assigned the unrealistic value of 6.0 GPa, the strains in the core remained below 2%. Evidently, the stresses transmitted to the core were limited by the flow stress of the jacket material. The result was that insufficient stresses, and consequently strains, were induced in the core material to predict failure. This is, of course, at odds with experimental observations.

One change that was implemented was a much finer mesh, as shown in Fig. 13a. Initially, a much simpler mesh was used; the mesh was a single mesh filled with the different materials (steel, gilding and lead). A more detailed mesh, one for each of the primary materials, provided for better stress resolution. But it was finally determined that the erosion strain for the jacket material was the controlling "numerical" parameter. As contrasted to large plastic deformation, it is believed that a better representation of the jacket–plate interaction might be one of gouging and cutting. This would suggest the use of a considerably lower "erosion" strain. A 10% erosion strain was used—instead of the typical 100–150%—for the jacket and lead materials, which resulted in contact between the core of the projectile and the target. Further, the jacket began to strip from the core (as observed in the experiments). Strains of a little over 2% were induced in the core at similar locations as the core-only simulations. Fig. 13b shows the configuration 24 μs after impact. The core is being stripped and the projectile is undergoing some damage close to the nose.

4. Experimental results

The results of seven experiments are summarized in Table 1. A picture of a broken core, from the impact against a 3.22-mm thick RHA plate, is shown in Fig. 14a. The fourth column of Table 1

Table 1
Summary of experimental test results

Test no.	Target material	Target thickness (mm)	Normalized hole diameter (h/R_p)	Core broken
423	RHA	3.22	0.34	Yes
428	RHA	3.22	0.66	Yes
425	RHA	3.22	1.00	Yes
574	6061-T6 Al	3.12	0.71	No
573	6061-T6 Al	3.12	0.89	No
569	6061-T6 Al	6.60	0.47	No
565	6061-T6 Al	6.60	0.94	No

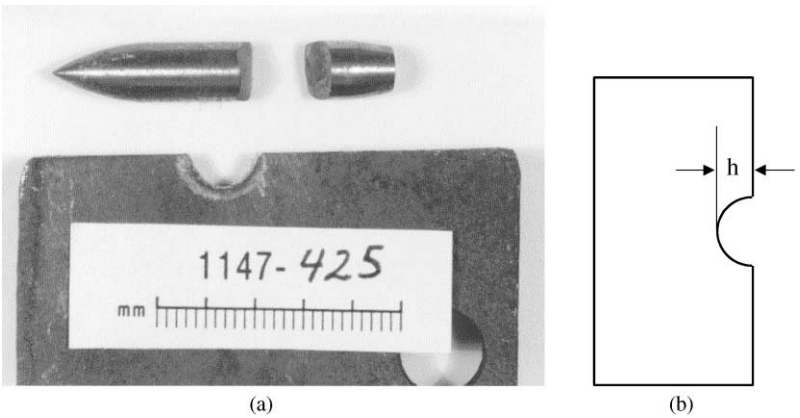

Fig. 14. (a) Photograph of fractured core; (b) nomenclature for hole measurement.

provides an indication of the overlap of the projectile with the plate. The distance h, see Fig. 14b, was measured. The radius of the core (3.09 mm) was used to normalize this distance, and is given in column 4 of Table 1.

For the three experiments where the core was fractured, the fracture occurred in the central region of the core, i.e., in the region between $\frac{1}{3}$ and $\frac{2}{3}$ the length of the core. Although failure can be somewhat of a stochastic process, experience with other types of experiments involving projectile fracture show that failure location is fairly reproducible if the exact impulsive loading location can be determined (for example, from flash radiography). Therefore, the variability in the exact fracture location is probably the result of differences in impact location (the relative overlap of the projectile with the target plate). The projectiles also do not fly perfectly straight—they have some pitch and yaw at impact—and this too could effect the fracture location. Additionally, there is considerable variability in the strain to failure from core to core as shown in Fig. 2. At this point, there are insufficient data to determine a causal relationship between fracture location and relative impact conditions.

Fig. 15. Photograph of bullet with aluminum plate.

The core was not fractured in any of the aluminum target plate tests. Very high speed digital images of the projectile–plate interaction show the projectile nose taking on an asymmetric extruded-like appearance, e.g. see Fig. 15, very similar to the numerical simulation results shown in Fig. 13b. It is concluded that interaction with the aluminum plate initiated the stripping process, but the jacket was not stripped in any of the aluminum plate experiments.

5. Conclusions

Projectile fracture is an effective defeat mechanism. An idealized analytical model was developed to provide initial insights into the conditions that would lead to fracture. The analytical model provided the basis for initial 3-D simulations, permitting efficient evaluation of mesh zoning requirements and interpretation of numerical results. The 3-D simulations were then extended to modeling the hard steel core of the 7.62-mm, armor-piercing, APM2 projectile. The results of the experiments combined with the calculated maximum strains shown in Fig. 12 suggest that computed axial strain must exceed 2% to achieve projectile fracture. This result is consistent with the stress–strain curves for the core material, Fig. 2. Numerical simulations of the entire APM2 projectile (core, lead nose, and jacket) suggest that the core must interact with the plate to induce fracture, i.e., a grazing impact that only involves the jacket is insufficient to fracture the core.

Simulations of the full projectile (jacket, lead nose, and core) showed that standard values for the erosion strain gave results that were incompatible with experiment for the plate-edge impact interaction. The erosion strain had to be considerably smaller to enable the core to interact with the target plate and induce sufficiently large strains that would then indicate fracture. Although we have attempted to "rationalize" this very small value by suggesting that the interaction process is one of gouging and cutting, instead of large-scale plastic deformation, this is admittedly conjecture. This area certainly requires further investigation.

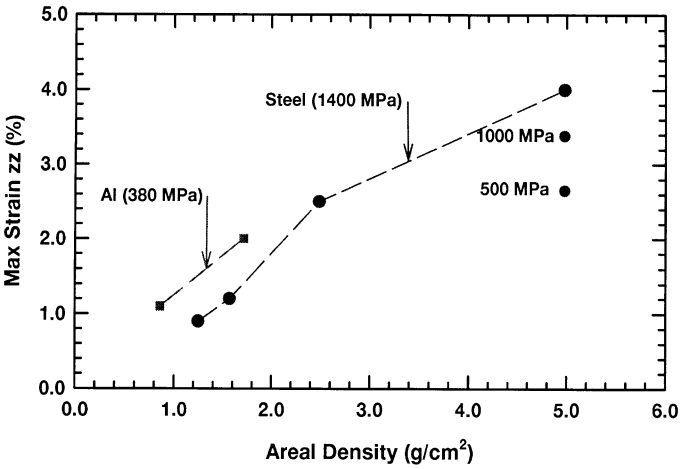

Fig. 16. Maximum strain in the core as a function of target areal density.

From Fig. 12, a steel plate, at the same thickness, is more effective than aluminum in fracturing the core. However, the results should be re-examined at the same target weight, i.e., areal density, which is the product of the target density and target plate thickness. The data plotted in Fig. 12 are shown in Fig. 16, but they are now plotted as a function of areal density. Although the 6.35-mm-thick aluminum plate did not fracture the core, the results of Fig. 16 suggest a slightly thicker aluminum plate would probably have fractured the core. Furthermore, on an equal areal density basis, 6061-T6 aluminum induces a larger strain than the high-hard (1400 MPa) steel plate. The results of Fig. 16 indicate that a minimum areal density of approximately $2\,g/cm^2$ is required to fracture the core.

Acknowledgements

This work was supported under contract DAAK60-97-C-9228 with the US Army Natick RD&E Center. The authors thank Ms. Janet Ward of Natick and Dr. Steve Wax of DARPA for their support and encouragement. S. Chocron would like to thank the Ministerio de Educación y Cultura of Spain for its financial support.

References

[1] Boley BA, Chao CC. Some solutions of the Timoshenko beam equations. J Appl Mech 1955;22:579–86.
[2] Cowper GR. The shear coefficient in Timoshenko's beam theory. J Appl Mech 1966;33:335.
[3] Century Dynamics. 1977. AUTODYN 3D Manual, Revision 3.0, Century Dynamics, San Ramon, CA.
[4] Kolsky H. Stress waves in solids. New York: Dover Publications, Inc., 1963.
[5] Johnson GR. 1998, Private communication.

[6] Johnson GR, Cook WH. 1983. A constitutive model and data for metals subjected to large strains, high strain rates and high temperatures. Proceedings of the Seventh International Symposium on Ballistics, The Hague, The Netherlands, pp 541–8.
[7] Johnson GR, Stryk RA. Eroding interface and improved tetrahedral element algorithms for high velocity impact computations in three dimensions. Int J Impact Engng 1987;5:411–21.